Available online at www.sciencedirect.com
SCIENCE DIRECT
Applied Catalysis A: General 298 (2006) 211–216
APPLIED CATALYSIS A: GENERAL
www.elsevier.com/locate/apcata

Deactivation of a precipitated iron Fischer–Tropsch catalyst—A pilot plant study

Dawid J. Duvenhage, Neil J. Coville *

Molecular Sciences Institute, School of Chemistry, University of the Witwatersrand, P.O. Wits, 2050 Johannesburg, South Africa

Received 10 June 2005; received in revised form 30 September 2005; accepted 7 October 2005
Available online 17 November 2005

Abstract

A pilot plant Fischer–Tropsch synthesis reaction was performed in a fixed bed reactor containing a precipitated iron catalyst. Sections were taken from the reactor and tested for Fischer–Tropsch activity in micro reactors. The catalyst sections were subjected to SEM, SIMS and XRD analysis and revealed catalyst deactivation due to (i) sulphur poisoning in the top portion of the reactor bed and (ii) magnetite formation and crystallite growth in the bottom portion of the reactor bed.

Keywords: Fischer–Tropsch; Deactivation; Iron catalyst; Sulphur poisoning; SEM

1. Introduction

Deactivation studies on Fischer–Tropsch (FT) catalysts have been undertaken since the first investigations were performed on these catalysts in the 1920s [1]. Since then there have been many articles written [2,3] and patents produced [4–6] on this topic. Indeed many elegant studies performed by Bukur [7], Davis [8], Bartholomew [9] and others have entailed long term investigations of FT catalysts using conditions that have simulated industrial reaction conditions. In recent times much effort has focussed on CSTR catalysts with most studies focussed on laboratory reactors [10–13]. From these results an understanding of the catalyst deactivation processes involved in the FT reaction has been obtained.

Some years ago we published [14] a report on the deactivation processes involved in a pilot plant study of the deactivation processes taking place over a typical precipitated iron catalyst [15]. These studies permitted an evaluation of the deactivation processes as a function of position in the reactor bed. In particular sulphur poisoning was shown to be important in the top section of the reactor while poisoning due to H_2O, formed in the F–T reaction, was shown to cause catalyst deactivation in the lower section of the catalyst bed. We now wish to complement these deactivation studies with data obtained from the use of scanning electron microscopy (SEM) and secondary ion mass spectrometry (SIMS) studies of the pilot plant catalyst. These techniques have been used previously by others for studying deactivation phenomena such as catalyst poisoning [16,17] and crystallite growth (sintering) [18,19]. Some information from our earlier study is highlighted herein to place the SEM and SIMS studies in context.

2. Experimental

A fixed bed pilot plant scale reactor was loaded with a precipitated iron catalyst synthesized by literature methods [15]. The catalyst was reduced and industrially purified synthesis gas (through the Rectisol process, to low ppb S levels) passed through the catalyst bed using typical industrial conditions for various periods of time [1,19]. The catalyst (20 fractions) were then unloaded and stored under nitrogen immediately before analysis or further use.

As mentioned in an earlier study [14], portions of each catalyst sample (~5 g) were also loaded into one of four laboratory micro reactors operated under identical experimental conditions. The catalysts were kept on line until the activity, as measured by the daily drainage of water and hydrocarbon products, had stabilized. Each of the laboratory

* Corresponding author.
E-mail address: ncoville@aurum.chem.wits.ac.za (N.J. Coville).

0926-860X/$ – see front matter © 2005 Elsevier B.V. All rights reserved.
doi:10.1016/j.apcata.2005.10.009

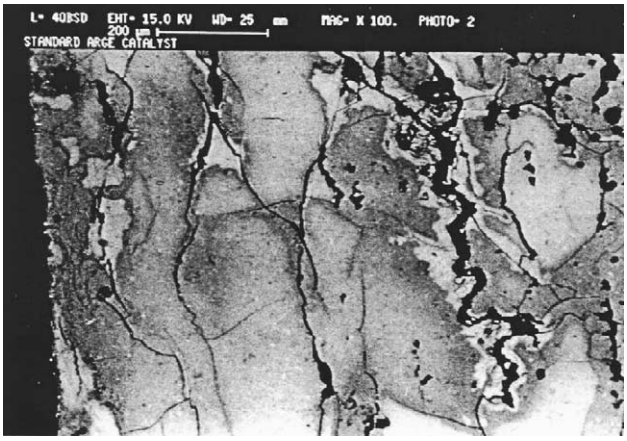

Fig. 1. SEM photograph of a reduced unused catalyst (×100).

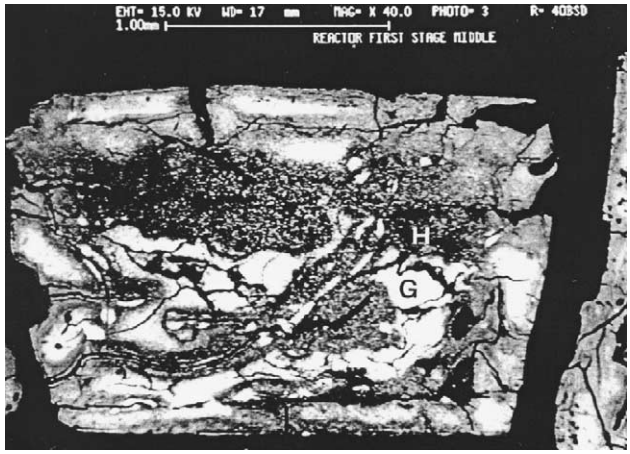

Fig. 3. SEM photograph of a used catalyst taken from one quarter from the top of the catalyst bed (×40).

micro reactors was tested with a known catalyst standard to establish both the data reproducibility and possible effects of the different reactors on the activity measurements. The different reactors gave results with relative differences of less than 3%.

Catalyst analysis by XRD, surface area and pore volume measurements as well as C and S elemental analyses was performed on the samples before and after use in the laboratory micro reactors as was discussed previously [14].

SEM photographs were obtained on a Cambridge Instruments 360 SEM fitted with a tungsten hair pin filament, energy dispersive analysis unit (EDAX) and link image analyzer (LIA), while secondary ion mass spectra and elemental mapping of the surface were recorded on a ESCALAB MK II equipped with a gallium gun (CSIR, Pretoria).

Representative samples from different bed fractions were taken for SEM and SIMS analysis. The samples analysed were: (i) a reduced unused catalyst (Fig. 1), (ii) a used sample from the top 10% of the reactor (Fig. 2), (iii) a used sample from the top 25% of the reactor (Fig. 3) and (iv) a used sample from the middle section of the reactor (Fig. 4).

3. Results

The pilot plant catalyst bed was unloaded in sections after different times on line as described previously [14]. The activity of each section was then determined in a micro reactor and the activity profiles as a function of position in the catalyst bed determined. The relative results (the activity is plotted relative to the fresh catalyst, i.e. a portion of the catalyst not used in the pilot plant study) are shown in Fig. 5 [14]. The inverted V shaped curve suggests two competing processes are occurring and that the catalyst deactivates with time.

The activity increased until a maximum activity was achieved about one quarter distance from the top of the reactor bed, followed by a gradual decrease in activity. Fig. 5 also indicates that the top section of the catalyst bed deactivates more rapidly than the bottom section of the reactor.

Sulfur analysis through the length of the catalyst bed indicated high levels to be present in the top section of the reactor (Fig. 6) [14].

SEM and SIMS studies on the catalysts revealed the magnetite concentration, and crystallite size, both increased

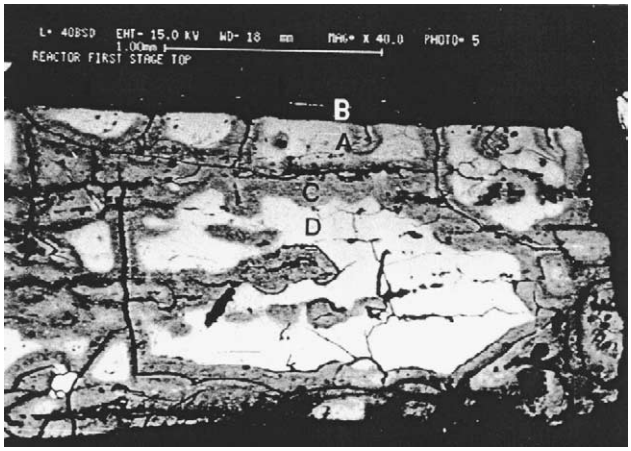

Fig. 2. SEM photograph of a used catalyst taken from the top section of a fixed bed reactor catalyst bed (×40).

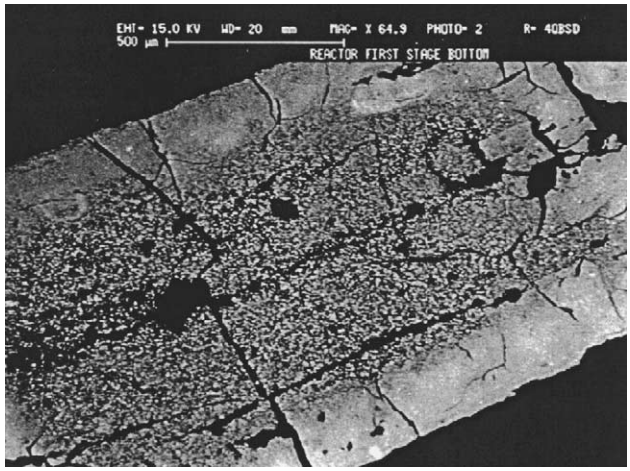

Fig. 4. SEM photograph of a used catalyst taken from the middle section of a fixed bed reactor catalyst bed (×40).

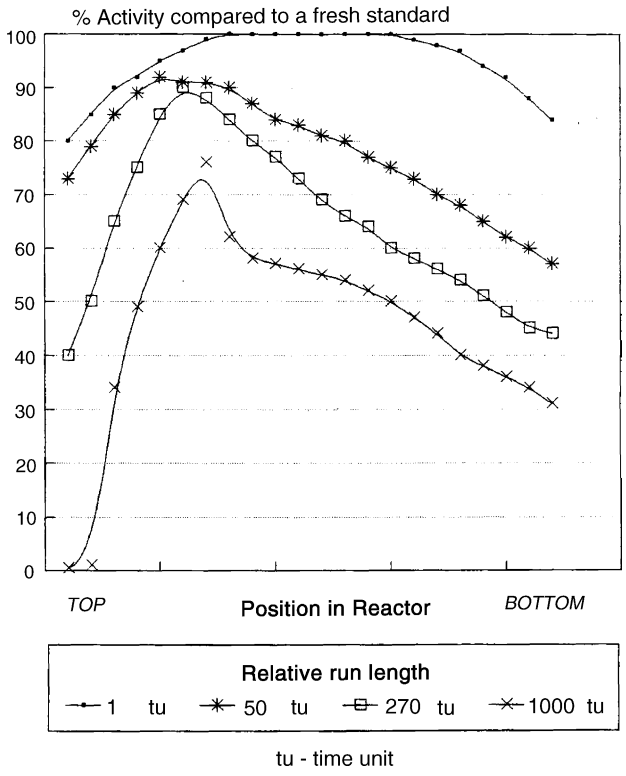

Fig. 5. Relative activity profile of iron precipitated catalysts after different periods of time on line, Times are in relative units (●, 1; *, 50; □, 270; ×, 1000).

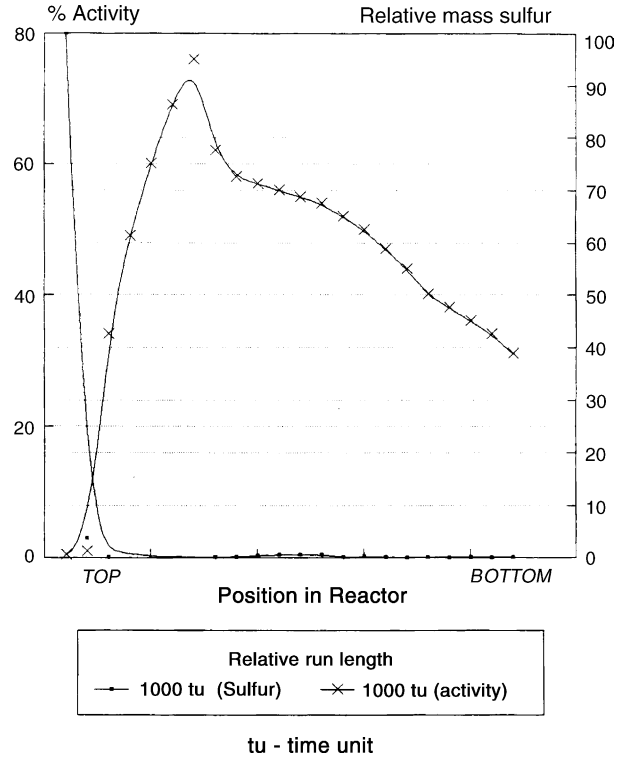

Fig. 6. Effect of sulphur on the relative activity profile of a fixed bed reactor catalyst (1000 time units) (×, activity; *, relative mass sulphur).

down the bed and with time on line as described previously [14].

4. Discussion

As shown in Fig. 5, the activity profile has an inverted V-shape in agreement with studies reported by Kolbe and Engelhard [19] on a related iron F–T catalyst. The results in Fig. 5 indicate that, as expected, the degree of deactivation increases with time on line [20]. The sulfur elemental analysis data are shown in Fig. 6 and indicates that sulphur is only observed in the top position of the reactor. The sulphur poisoning arises from ppb levels of sulphur impurities found in the synthesis gas [1,19,21]. It is apparent from the results that the top portion of the reactor is acting as a "guard bed" to remove this impurity. The XRD analysis of the catalyst samples shows the presence of magnetite in all the catalyst sections.

To further substantiate the role of sulfur a dual reactor system was used [14]. In this set of experiments two pilot plant reactors were connected in series. Each reactor was half filled with catalyst and half filled with inert ceramic spheres. The tail gas from the first reactor was fed into the second reactor after condensable products (H_2O, liquid products) had been removed. Following reaction, the catalyst was unloaded in sections from both reactors under inert conditions as described for the study involving the single reactor.

4.1. SEM analysis

4.1.1. Reduced, unused catalyst (Fig. 1)

This catalyst was analysed for comparative purposes. As can be seen, the catalyst displays a smooth surface with fine cracks, possibly formed during the reduction process. SEM-EDAX analysis revealed a homogeneous distribution of the iron throughout the catalyst section.

4.1.2. Used sample, top 10% of the reactor (Fig. 2)

A dramatic change in the physical appearance of the catalyst is to be noted. The SEM photograph (×40 magnification) reveals a thin bright outer rim next to a black rim (B). Grey areas (A, C) mostly observed along the strong cracks leading to the pellet interior are also seen. Finally, a bright section (D) is observed in the interior of the pellet.

An enlargement (×200) of the grey area (Fig. 2, A) is shown in Fig. 7 and an enlargement (×2000) of Fig. 7 position B is shown in Fig. 8. A SEM-EDAX analysis of the bright region in Fig. 8 was performed and indicated this region consisted mainly of iron and sulphur. SIMS analysis of the same region also indicated similar results (see below).

SEM-EDAX analysis was performed on the positions C, D, E and F in Fig. 7. The analysis of the grey area along the crack, close to D, indicated that it was rich in iron, carbon and oxygen, (and low levels of sulfur were detected; also see section on SIMS analysis) while the region marked F was found to be rich only in oxygen and iron.

It is known that synthesis gas diffuses into the porous catalyst pellets during the F–T reaction. The resulting reactions

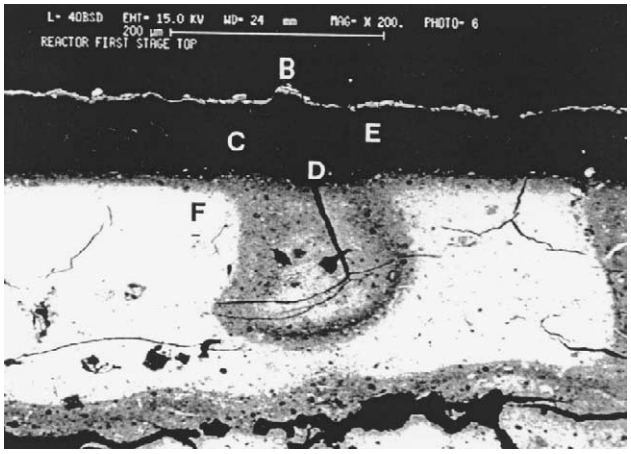

Fig. 7. Enlargement of the grey area marked A in Fig. 2 (×200).

in the pores lead to the formation of H_2O and CO_2 [14]. This implies that the initial reducing gas (CO/H_2) progressively becomes more oxidizing as it penetrates into the catalyst. Further, through interaction of the CO (or CO_2) with the iron, iron carbides form and these carbides would be expected to form along the catalyst cracks. This finding is in agreement with data reported by Chaffee et al. [22] on a Fe/Mn catalyst.

In summary, the catalyst pellet after reduction comprises of three distinct regions: (a) a rim of iron sulphide, (b) regions next to cracks in the catalyst rich in iron carbides and some sulphur and (c) a catalyst interior comprising of iron oxides.

4.1.3. Used catalyst, 25% from the top of the reactor (Fig. 3)

In Fig. 3 the physical nature of the catalyst is again seen to be different. In this Figure no bright or black outer rim is observed. A larger portion of the catalyst interior is grey in appearance and fewer bright spot are observed. The catalyst has become more granular.

As expected, SEM-EDAX analysis revealed no sulphur in the rim. Further, the analysis revealed the presence of Fe and O in area G, and Fe, O and C in area H. This data is thus consistent with the data in (ii) above. The granular texture is discussed below.

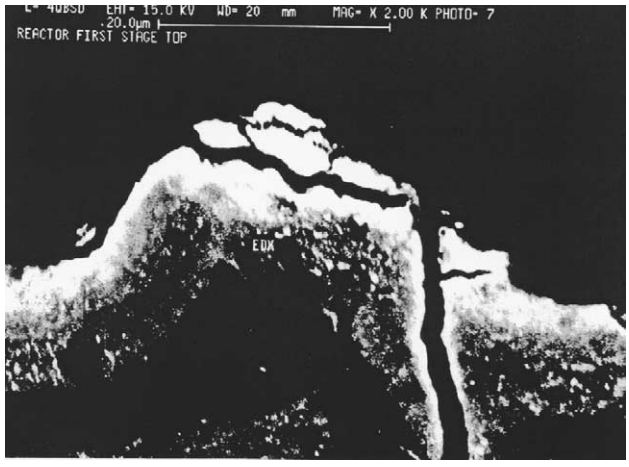

Fig. 8. Enlargement of the black area marked B in Fig. 5 (×2000).

4.1.4. Used catalyst, middle section of the reactor (Fig. 4)

In this catalyst pellet a smooth outer rim and granular interior, displaying large quantities of small bright spots are noted. SEM-EDAX analysis again confirmed that the bright areas were iron rich, while the grey areas contained iron, oxygen and carbon.

An important feature that can readily be observed in Figs. 1–4 is the increase in granular appearance of the pellets with position in the reactor. This is related to the growth of iron oxide crystallites down the catalyst bed [23–25] and is highlighted by a further consideration of the catalyst pellet. Magnification (×6000) of the middle section of the used catalyst (Fig. 9) and SEM-EDAX analysis of regions A and B were performed. The grey product (area A) is rich in oxygen and lean in carbon, and it is therefore believed that mostly iron oxide and no iron carbide is present. The brighter areas (area B) are rich in iron. Again it is suggested that the presence of carbon and oxygen correlate with the presence of iron oxide and iron carbide.

Finally, SEM-LIA analysis of the particles found in the three sections of the catalyst bed revealed that an increase in the iron phase is observed with bed depth. Fig. 10, position A–C, show the size of the particles constituting the bright areas in the top 10%, 20% and 50% of the catalyst bed (×7000 magnification) and clearly indicates the increase in the iron crystallite size down the reactor. Indeed a near linear increase in average diameter of the metal particles down the reactor bed is observed. This relation was also confirmed by XRD analysis of the same catalysts as reported previously [14].

A dual reactor study was undertaken to confirm the results of the single reactor study. The key feature in this experimental arrangement was that both predicted deactivation reagents (H_2O, S) were removed before the feed stream entered the second reactor [14]. Further, by using two half-filled reactors comparison could be made with the single reactor study. A detailed analysis of the activities of the dual reactor shows that the first reactor (single, dual reactors) gives a decline in activity earlier than in the second reactor. This difference in behaviour

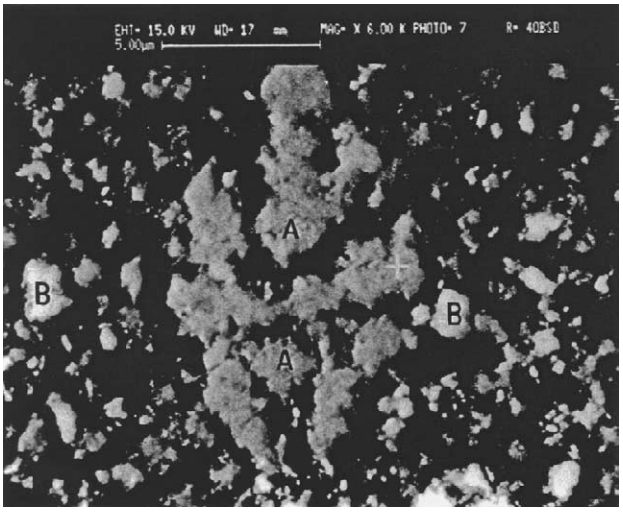

Fig. 9. SEM photograph of a catalyst pellet showing the middle section of the catalyst bed (×6000): (A) rich in oxygen and lean in carbon; (B) rich in iron.

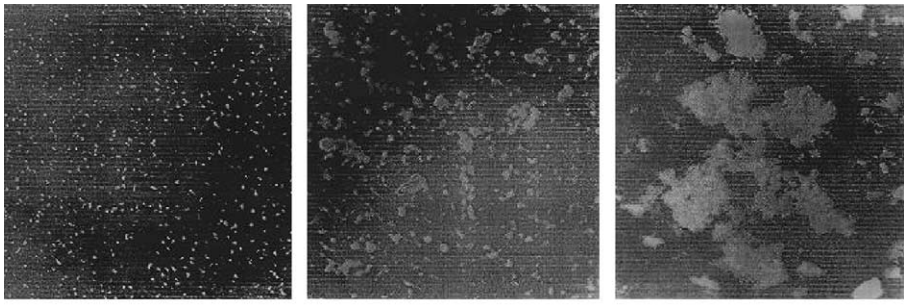

Fig. 10. (A) Magnification of the bright areas (iron crystallites) from the top section of the catalyst bed (×7000); (B) magnification of the bright areas (iron crystallites) from the most reactive section of the catalyst bed (×7000); (C) magnification of the bright areas (iron crystallites) from the middle section of the catalyst bed (×7000).

relates to the lower concentration of the reactor feed in the second of the two reactors. Thus it is anticipated that the rate of H_2O formation will be lowered in the second reactor and that this would delay the onset of oxidation, as is observed. Both reactors show a definite drop in the catalyst activity due to the unreactive oxide phases and to the hydrothermal sintering of the catalyst. Both these deactivation processes are expected in the two reactors connected in series, and the effect is predicted to increase down the catalyst bed, as the partial pressure of water increases. This is observed.

Both reactors showed an equivalent increase in magnetite concentration through the reactor bed [14]. The relative crystallite size, as well as BET surface area, and pore volumes for the samples from both stage reactors are similar. It is thus apparent that the sulphur plays no part in the magnetite formation.

4.2. SIMS analysis

The SIMS technique has a much higher sensitivity than SEM-EDAX and can hence detect sulphur at the ppm level. Ion mass spectra of the outer rim (area marked "B" in Fig. 2), the grey areas next to the cracks (area marked "C" in Fig. 2) and the bright areas in the interior of the catalyst pellet (area marked "D" in Fig. 2) were recorded. SIMS analysis of the catalyst pellet showed the sulphur concentration to be high on the outer surface and not detectable in the interior of the catalyst, and that sulphur, in concentrations similar to that of the outer surface, were found along the cracks leading to the interior of the catalyst pellet. These results show that the loss of catalytic activity due to poisoning is only a result of the poisoning of the catalyst surface and cracks and not a consequence of bulk catalyst poisoning. This result is similar to that obtained by most other researchers in the field of catalyst poisoning [17,22,26,27].

Finally, a negative ion mass spectral analysis of the catalyst pellet revealed [28] the presence of large quantities of sulphur, oxygen and carbon chains (from hydrocarbon products not completely extracted from the catalyst) and contaminant impurities such as chloride and fluoride obtained from the carbon extraction process.

4.3. XRD analysis [14]

Oxidation of the reactive iron metal phase to give unreactive magnetite (Fe_3O_4) phase as detected by XRD and iron crystallite growth occurs during the FT reaction. Hagg's carbide (Fe_5C_2) as detected by XRD was found predominantly in the top part of the reactor. It was observed that the amount of magnetite increased with catalyst time on line, e.g. the magnetite concentration doubled on increasing the time on line four-fold.

The magnetite concentration also increased down the catalyst bed [14]. This phenomenon can be explained by the increase in water partial pressure and hence the oxidizing nature of the gas atmosphere down the reactor. A similar phenomenon was observed by Kolbel and Engelhard [19]. Catalyst oxidation thus appears to contribute significantly to the drop in catalytic activity.

A thorough XRD investigation was undertaken of the catalysts used in the dual reactor study. The Fe_3O_4 phase was identified as magnetite (lattice constant 8.40 Å) although maghemite (y-Fe_2O_3; with lattice constant 8.35 Å) may be present. This phase increased down the reactor bed. Hagg's carbide Fe_5C_2 was present throughout the length of the reactor. From the middle of the catalyst bed a second carbide phase (cementite, Fe_3C) was also detected, but its concentration showed no trend down the catalyst bed.

Simultaneously there is a marked decrease in the total surface area and an increase in the pore volume of the catalyst with bed depth. The crystallite size of the catalyst particles, as determined by XRD measurements, was found to increase with time on line [14,18]. It is well known that water can adsorb into metal oxides as a first step in the process of metal crystallite growth, an effect that would readily rationalize our data [29]. Although a direct correlation between activity and the number of catalyst active sites is expected, the relationship between active sites and crystallite size is not expected to be linear.

5. Conclusions

The SEM and SIMS analysis of a typical industrial catalyst tested in a pilot plant reactor has clearly indicated the processes

that are responsible for catalyst deactivation in a fixed bed Fischer–Tropsch reactor. These are sulphur poisoning in the top part of the reactor and crystallite growth (sintering) in the lower portion of the reactor bed. The results are entirely consistent with our earlier reactor study results [14].

Acknowledgements

We wish to thank SASTECH Research and Development for financial support. We would also like to acknowledge the valuable input of Dr. Mark Dry and Dr. Rafael Espinoza in the study.

References

[1] M.E. Dry, Catal. Sci. Technol. (1981) 1159.
[2] H. Schulz, Appl. Cat. A. Gen. 186 (1999) 3.
[3] C.H. Bartholomew, in: L. Guczi (Ed.), New Trends in CO Activation, Elsevier, Amsterdam, 1991 (Chapter 5).
[4] Sasol Technology (Propriety) Limited, USA Patent 6,265,452 (2001).
[5] Exxon Research and Engineering Company, USA Patent 4,624,968 (1986).
[6] Shell Oil Company, USA Patent 4,472,534 (1984).
[7] W. Ma, Y. Ding, V.H. Carreto Vázquez, D.B. Bukur, Appl. Catal. A. Gen. 268 (2004) 99.
[8] N. Sirimanothan, H.H. Hamdeh, Y. Zhang, B.H. Davis, Catal. Lett. 82 (2002) 181.
[9] C. Bartholomew, Appl. Catal. 212 (2001) 17.
[10] T.J. Donnelly, C.N. Satterfield, Appl. Catal. 56 (1989) 231.
[11] D.B. Bukur, W.-P. Ma, Victor Carreto-Vazquez, Topics Catal. 32 (2005) 135.
[12] P.J. van Berge, J. van de Loosdrecht, S. Barradas, A.M. van der Kraan, Catal. Today 58 (2000) 321.
[13] B.H. Davis, Topics Catal. 32 (2005) 143.
[14] D.J. Duvenhage, R.L. Espinoza, N.J. Coville, in: B. Delmon, G.F. Froment (Eds.), Catalyst Deactivation Studies in Surface Science and Catalysis, vol. 88, Elsevier Science B.V., 1994, p. 351.
[15] C.D. Frohning, Fischer–Tropsch Synthesis, in: J. Falbe (Ed.), Chemierohstoffe aus Kohle, Thieme, Stuttgart, 1977.
[16] R.J. Madon, H. Shaw, Catal. Rev. Sci. Eng. 15 (1977) 70.
[17] P.K. Agrawal, W.D. Fitzharris, J.R. Katzer, in: B. Delmon, G.F. Froment (Eds.), Catalyst Deactivation, vol. 179, Elsevier Science Publishers B.V., Amsterdam, 1980.
[18] E. Ruckenstein, Metal–Support Interactions in Catalysis Sintering and Redispersion, Van Nostrand Reinhold Company, New York, 1987 , pp. 230–236, 239–241, 271, 287, 291–294, 296.
[19] H. Kölbel, F. Engelhard, Erdöl und Kohle, 3, 11, 529 (1950).
[20] S.A. Eliason, C.H. Bartholomew, Appl. Catal. 186 (1999) 229.
[21] Z.-T. Liu, Y.-W. Li, J.-L. Zhou, Z.-X. Zhang, B.-J. Zhang, Appl. Catal. 161 (1997) 137.
[22] A.L. Chaffee, I. Campbell, N. Valentine, Appl. Catal. 47 (1989) 253.
[23] E. Ruckenstein, D.B. Badyburjor, J. Catal. 48 (1977) 73.
[24] E. Ruckenstein, B. Pulvermacker, J. Catal. 29 (1973) 224.
[25] D.D. Dadyburjor, in: B. Delmon, G.F. Froment (Eds.), Catalyst Deactivation, vol. 21, Elsevier Science Publishers B.V, Amsterdam, 1987.
[26] S. Berkmann, J.C. Morrell, G. Egloff, Catalysis Inorganic and Organic, vol. 372, Reinhold Publishing Corporation, New York, 1940.
[27] J.F. Schultz, F.S. Karn, R.B. Anderson, U.S. Bur. Mines, Rep. Invest., 6974 (1967) (as reported by R.J. Madon, H. Shaw, Catal. Rev. Sci. Eng., 15 (1977)).
[28] D.J. Duvenhage, MSc. Thesis, University of the Witwatersrand, Johannesburg, South Africa, 1990.
[29] D.A. Dowden, in: J.L. Figueiredo (Ed.), Progress in Catalyst Deactivation, Martinus Nijhoff Publishers, The Hague, 1982, p. 283.